SPINTRONICS

Dramatic influence of curvature of nanowire on chiral domain wall velocity

Chirag Garg,[1,2,3]* See-Hun Yang,* Timothy Phung,[2] Aakash Pushp,[2] Stuart S. P. Parkin[1,2,3]†

The use of current pulses to move domain walls along nanowires is one of the most exciting developments in spintronics over the past decade. We show that changing the sign of the curvature of a nanowire changes the speed of chiral Néel domain walls in perpendicularly magnetized nanowires by up to a factor of 10. The domain walls have an increased or decreased velocity in wires of a given curvature, independent of the domain wall chirality and the sign of the current-induced spin-orbit torques. Thus, adjacent domain walls move at different speeds. For steady motion of domain walls along the curved nanowire, the torque must increase linearly with the radius, which thereby results in a width-dependent tilting of the domain wall. We show that by using synthetic antiferromagnetic nanowires, the influence of the curvature on the domain wall's velocity is eliminated, and all domain walls move together, emphasizing the use of such structures for spintronic applications.

INTRODUCTION

Early interest in the manipulation of magnetic moments by torques derived from spin angular momentum transfer (*1*, *2*) focused on spin-polarized tunneling currents that are the basis for the writing of magnetic memory elements in magnetic random access memories (*3*, *4*) and spin-dependent scattering-induced spin-polarized currents, which can be used to manipulate domain walls (DWs) (*5*–*11*). More recently, it has been realized that significant spin currents can be generated from electrical currents via the spin Hall effect (SHE) in metals and alloys (*12*, *13*). Such spin currents can be used to apply spin-orbit torques to rotate the magnetization of magnetic elements or to move chiral Néel DWs (*14*–*17*) and skyrmions (*18*, *19*). Recently, the lock-step motion of a series of DWs with speeds of up to ~1000 m/s has been observed (*14*, *20*, *21*). However, nearly all experiments to date on the current driven motion of DWs in magnetic nanowires have focused on straight nanowires. Here, we show that the curvature of nanowires strongly affects the velocity of the DWs, so that they no longer move in lockstep.

Experiments were performed on devices (Fig. 1A) that were formed from ultrathin Co/Ni/Co sandwiches deposited on a Pt underlayer (Fig. 1, B, D, and E) with, in some cases, a Pt overlayer. The Pt under- and overlayers induce perpendicular magnetic anisotropy (PMA) in the Co/Ni/Co sandwich and also, most importantly, give rise to a Dzyaloshinkii-Moriya interaction (DMI) (*22*–*24*) that stabilizes Néel DWs that are chiral in nature. Thus, DWs are formed at the boundaries between magnetic regions with magnetization pointing out of (⊙) and into the plane (⊗) of the nanowire, where the magnetization rotates from ⊙ to ⊗ in a plane that is perpendicular to the length of the DW. This rotation can be in a clockwise or counterclockwise sense, which is determined by the sign of the DMI vector. By tuning the Pt/Co interface, we are able to tune the direction of the dominant DMI to change the chirality of the DW as well as the magnitude and sign of the SHE (Fig. 1, B, D, and E) (*20*, *25*). The chiral spin torque is largely determined by the DMI and SHE (*14*). A typical device is U-shaped, allowing direct comparisons of the measured DW velocity in the straight and curved sections for the same current pulses. For the curved section, the distance traveled by the DW along the arc q, where the mean radius, R, across the wire width is used for calculating the DW velocity, v. The curvature of the nanowire is defined as $|\kappa| = \frac{1}{R}$, and the sign of the curvature is defined with respect to the direction of motion of the DW. If the DW moves along a clockwise path, then $\kappa > 0$, and if it moves along a counterclockwise path, then $\kappa < 0$. [Note that, the curvature can be defined equally well in the same way with respect to the current direction (see the Supplementary Materials).] We assign DWs as either ⊙ | ⊗ or ⊗ | ⊙ with regard to the direction of their motion. The injection procedures for a single DW or a pair of DWs are described in the Supplementary Materials.

RESULTS

The dependence of the v on the current density J is shown in Fig. 1B for a device with $R = 7$ μm and wire width $w = 2$ μm. Results are compared for the DW motion in the straight and curved sections of the same device for different curvatures and for ⊙ | ⊗ and ⊗ | ⊙ DWs. It is clear that ⊗ | ⊙ DWs for positive curvature and ⊙ | ⊗ DWs for negative curvature move much faster than the same DWs in the straight section (where ⊙ | ⊗ and ⊗ | ⊙ DWs move at the same speed). When the sign of the curvature is switched, the corresponding DWs move much more slowly. The ratio of the DW speeds for opposite curvatures can reach more than 300% of the lower speed in Fig. 1B.

The dependence of DW velocity on curvature is shown more vividly by concurrently studying the motion of a pair of DWs. Typical results from the same device used in Fig. 1B are shown in Fig. 1C. Two DWs with varying inter-DW distances were initially injected into the curved section of the wire. Then, two current pulses, each with a length of 100 ns and a current density of 0.6×10^8 A/cm^2, were applied to move the two DWs. The four panels in Fig. 1C correspond to the four cases for ⊙ | ⊗ | ⊙ and ⊗ | ⊙ | ⊗ DWs for the two different curvatures. The two DWs are color-coded in each image, and their respective motions are represented by curved arrows of the same corresponding color. In each case, the DWs move at different velocities, which is manifested in the Kerr difference images as an expansion or contraction of the initial spacing between the DWs. Consistent with the single DW data shown in Fig. 1B, we find that (i) ⊗ | ⊙ DW with positive curvature moves at the same high speed as the ⊙ | ⊗ DW with negative curvature (Fig. 1B, compare top left and bottom right panels) and that (ii) ⊙ | ⊗ DW with positive curvature moves at the same low speed as the ⊗ | ⊙ DW with negative curvature (Fig. 1B, compare top left and bottom right panels).

[1]Max Planck Institute for Microstructure Physics, Halle (Saale) D-06120, Germany. [2]IBM Research–Almaden, San Jose, CA 95120, USA. [3]Institute of Physics, Martin Luther University Halle-Wittenberg, Halle (Saale) D-06120, Germany.
*These authors contributed equally to this work.
†Corresponding author. Email: stuart.parkin@mpi-halle.mpg.de

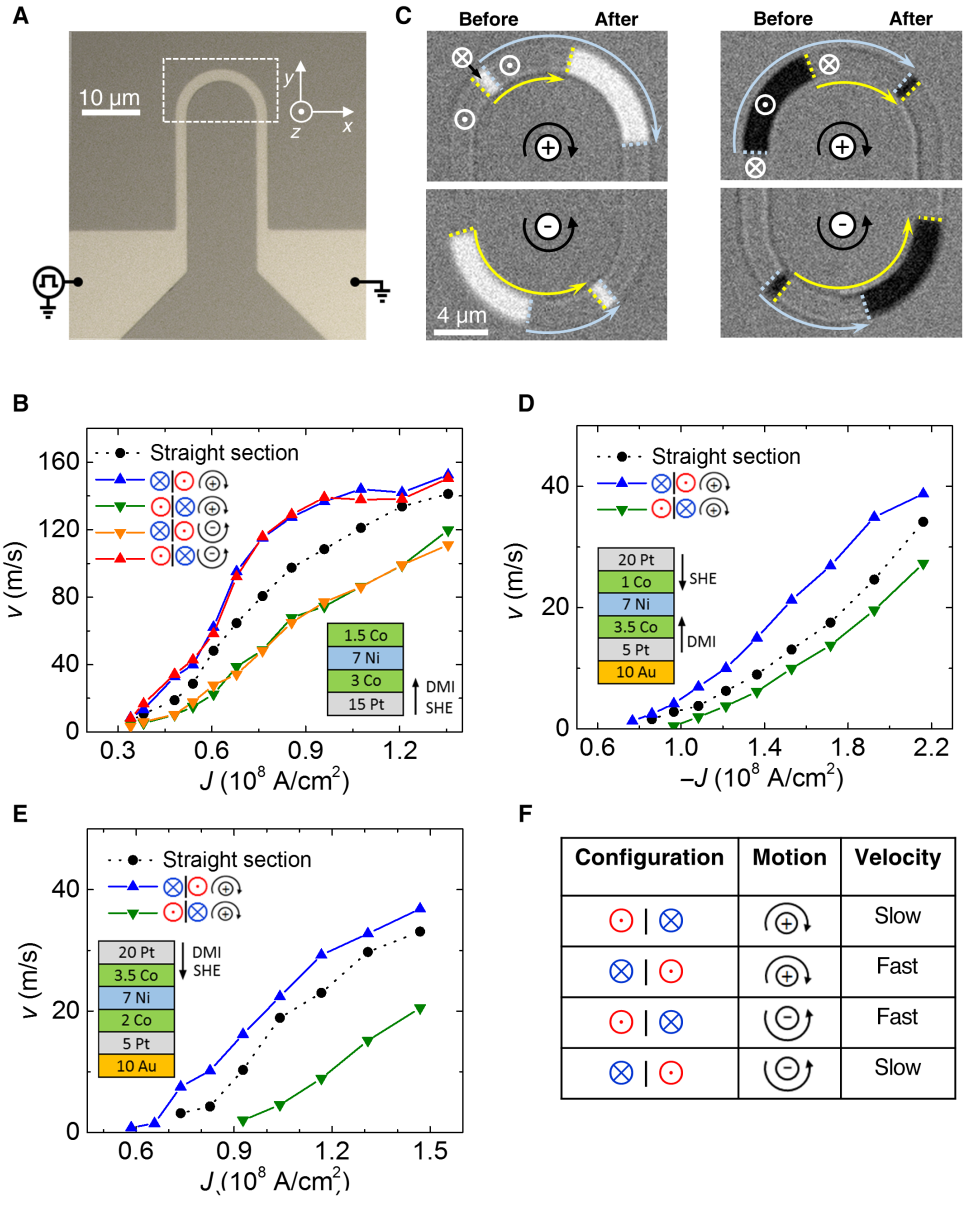

Fig. 1. Dependence of the DW velocity on curvature for different structures. (**A**) Optical image of a typical U-shaped device with $R = 7$ μm and $w = 2$ μm. (**B**) v versus J shows faster or slower DW motion in a curved nanowire compared to a straight wire. (**C**) Representative Kerr images showing the expansion or contraction of a magnetic domain along the positive or negative curvature of a curved nanowire. The Kerr images are taken before and after the application of two 100-ns-long electrical pulses with a current density of 0.6×10^8 A/cm^2. They are overlaid together, and the unedited picture is available in fig. S14. The yellow (gray) dots indicate the positions of ⊙ | ⊗ (⊗ | ⊙) DWs, and the arrows represent the trajectory of their motion. (**D** and **E**) v versus J showing the same relationship [as (B)] between the sign of the curvature on the increase or decrease in the DW velocity irrespective of the signs of DMI and SHE. (**F**) Truth table derived on the basis of (B), (D), and (E). Note that thicknesses of the layers in (B), (D), and (E) are in angstrom.

In Fig. 1 (D and E), we compare similar Co/Ni/Co structures in which variations in thicknesses of the Pt and Co layers at the top and bottom interfaces are used to control the effective signs of the DMI and SHE in the structures (*20*, *25*). Our experiments show that for any values of SHE and DMI, ⊗ | ⊙ (⊙ | ⊗) DWs go faster (slower) for positive curvature. Conversely, ⊗ | ⊙ (⊙ | ⊗) DWs go slower (faster) for negative curvature. Thus, although the motion of DWs in such structures arises from two chiral phenomena, namely, DMI and SHE, the chirality of these phenomena plays no role in determining whether the DWs go faster or slower for a given curvature. This is summarized in Fig. 1F.

The dependence of the DW velocity on the radius of curvature and width of the nanowire is shown in Fig. 2. We find that whether the DW velocity is increased or decreased for a given curvature is independent of R and w. We note that there is a threshold current density J_c needed to cause DW motion, as shown in Figs. 1 (B, D, and E) and 2 (A and D). When J slightly exceeds the threshold current for DW motion, the ratio of the velocities for ⊙ | ⊗ (UD) and ⊗ | ⊙ (DU) DWs for the same curvature $\left(\frac{v_{DU}}{v_{UD}}\right)$ takes the largest value, reaching almost 10 for the smallest R used in our experiments, as shown in Fig. 2B. However, when J is increased significantly above J_c, $\frac{v_{DU}}{v_{UD}}$ becomes smaller but remains larger than 1 and becomes insensitive to R and w. We suppose

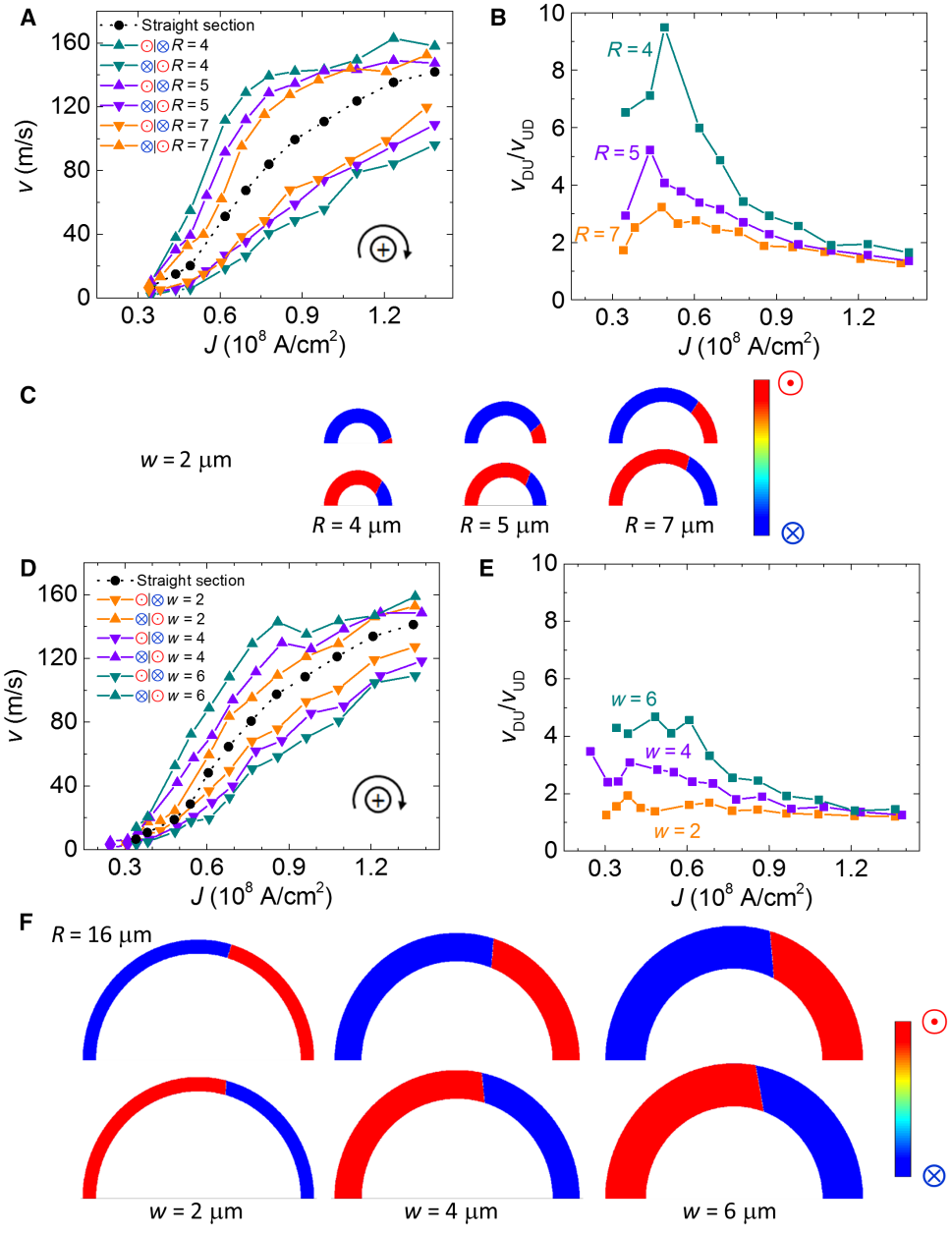

Fig. 2. Influence of curvature and width of the wire. DW motion as a function of the magnitude of the curvature (**A** to **C**) and width (**D** to **F**) for the film structure used in Fig. 1B. (C and F) The analytical model simulations for ⊗ | ⊙ (top) and ⊙ | ⊗ (bottom) DW displacements in their respective wires after a 40-ns current pulse with current density of 1.2×10^8 A/cm^2 is applied. (C) shows images for representative wires with various R for a fixed $w = 2$ μm, and (F) shows images for various w for $R = 16$ μm. The DW's initial position is at the center of each nanowire. (A) and (D) show v versus J. (B) and (E) show the calculated ratio ($\frac{v_{DU}}{v_{UD}}$) of the ⊗ | ⊙ and ⊙ | ⊗ velocities for the same J.

that the motion of the DWs at low current densities will be "creep-like," that is, dominated by thermal activation, and at higher current densities will be "flow-like." Then, the current density at which the DW motion passes from one regime to the other can be influenced because of the enhanced or reduced torques resulting from the curvature of the wire. In their respective regimes, the ratio of the curvature-dependent torques is similar. Thus, the peak in the velocity ratio will appear when the faster DW moves from the creep-like to the flow-like regime. Our quasi–two-dimensional (2D) analytical model of the DW motion that we discuss below includes thermal effects, and when we include a periodic pinning potential, we find a similar peak in the velocity ratio we find experimentally.

DISCUSSION

Previously, to gain an understanding of the motion of DWs in response to spin-orbit torques, it has proven to be very insightful to use an analytical 1D model in which the DW's profile is assumed unchanged (*14*, *26*). Here, we develop a quasi-2D model for curved wires under the assumption that the DW's profile now remains constant within the DW's moving frame of reference. To do this, we need to make a transformation between the Cartesian coordinate system of the observer and the cylindrical coordinate system of the DW. The critical parameters in the model to describe the DW motion with the moving frame of reference are q, ϕ, and ζ (see Fig. 3A and fig. S1A). ϕ is

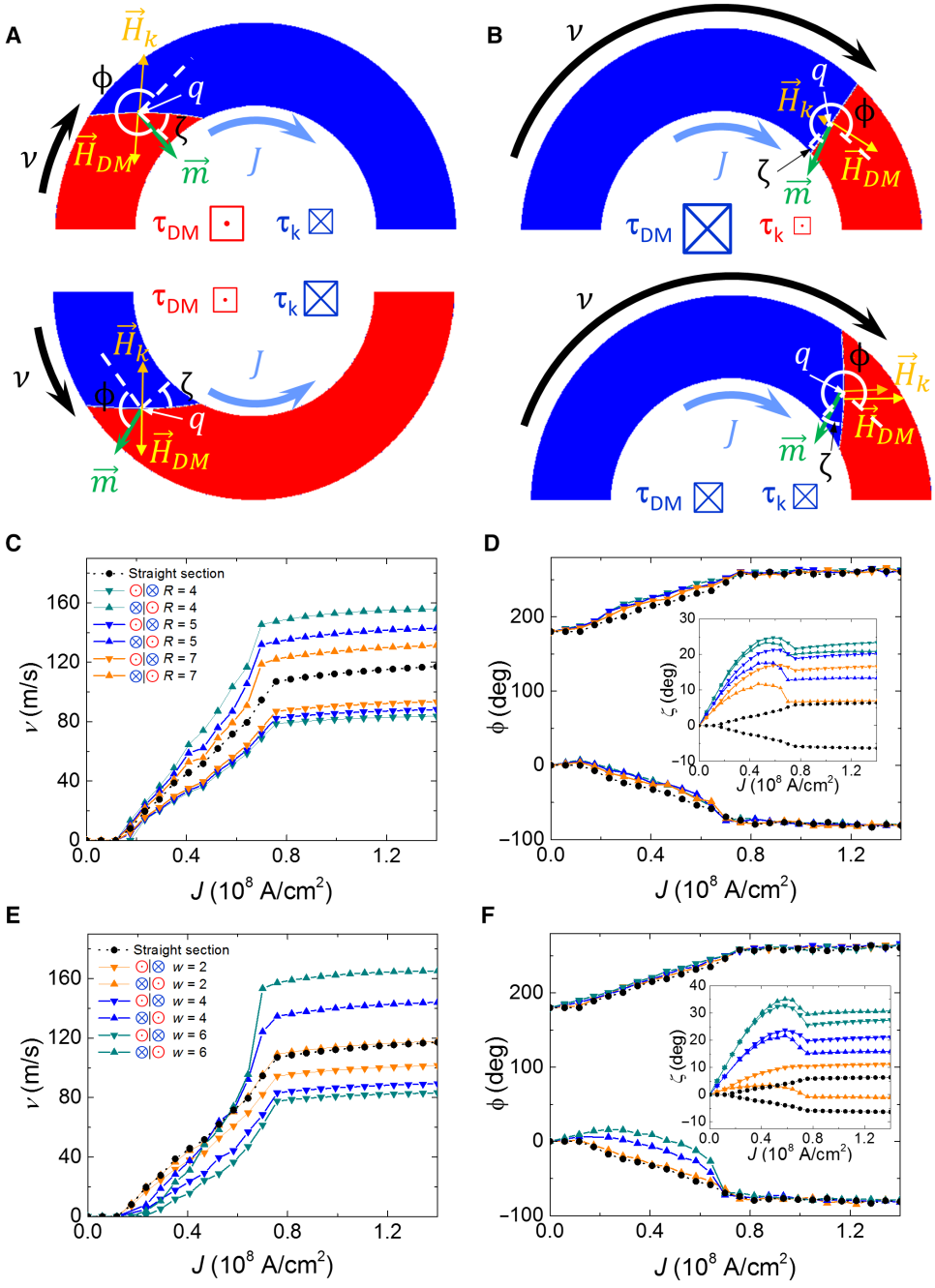

Fig. 3. A quasi-2D model simulation of the CIDWM in curved nanowires. (**A** and **B**) Schematic illustration of the critical parameters, fields, and torques that describes the current-induced DW motion (CIDWM). (A) ⊙ | ⊗ with positive curvature (top) and ⊗ | ⊙ with negative curvature (bottom). (B) ⊗ | ⊙ with positive curvature at low *J* (top) and ⊗ | ⊙ with positive curvature at high *J* (bottom). Size of symbols ⊡ and ⊠ represent the magnitudes of their respective torques. (**C** and **E**) Calculated *v* versus *J* for ⊙ | ⊗ and ⊗ | ⊙ configurations: (C) straight wire and curved wires with *R*= 4, 5, and 7 μm for a fixed *w* = 2 μm; (E) straight wire and curved wires with *w* = 2, 4, and 6 μm for a fixed *R* = 16 μm. (**D** and **F**) Calculated ϕ (main panels) and ζ (insets) versus *J* that correspond to (C) and (E), respectively, with the same corresponding colors and symbols. See fig. S11 for details about the parameters used in the calculations. Note that *R* and *w* in (C) to (F) are in micrometers.

the angle that the net magnetization of the DW, $\vec{m}$, makes with respect to the tangent direction to the nanowire, and ζ is the tilting angle of the DW with respect to the radial direction. $\vec{H}_{DM}$ is the DMI exchange field whose direction is always perpendicular to the DW, and $\vec{H}_k$ is the DW shape anisotropy field, which is also always perpendicular to the DW, but whose direction favors $\vec{m}$ being parallel to the DW. There are two important torques that drive the DW, as shown in Fig. 3A. These torques derived from $\vec{H}_{DM}$ and $\vec{H}_k$ are $\vec{\tau}_{DM} = -\gamma \vec{m} \times \vec{H}_{DM}$ and $\vec{\tau}_k = -\gamma \vec{m} \times \vec{H}_k$, respectively, where γ is the gyromagnetic ratio.

The most important factor that changes the DW velocity in curved wires compared to that in straight wires is the current-induced tilting of the DW from its initial radial direction that it takes up in the absence of current. Current-induced tilting of DWs in straight nanowires has previously been observed (*27*, *28*) and is due to an increase in the DMI

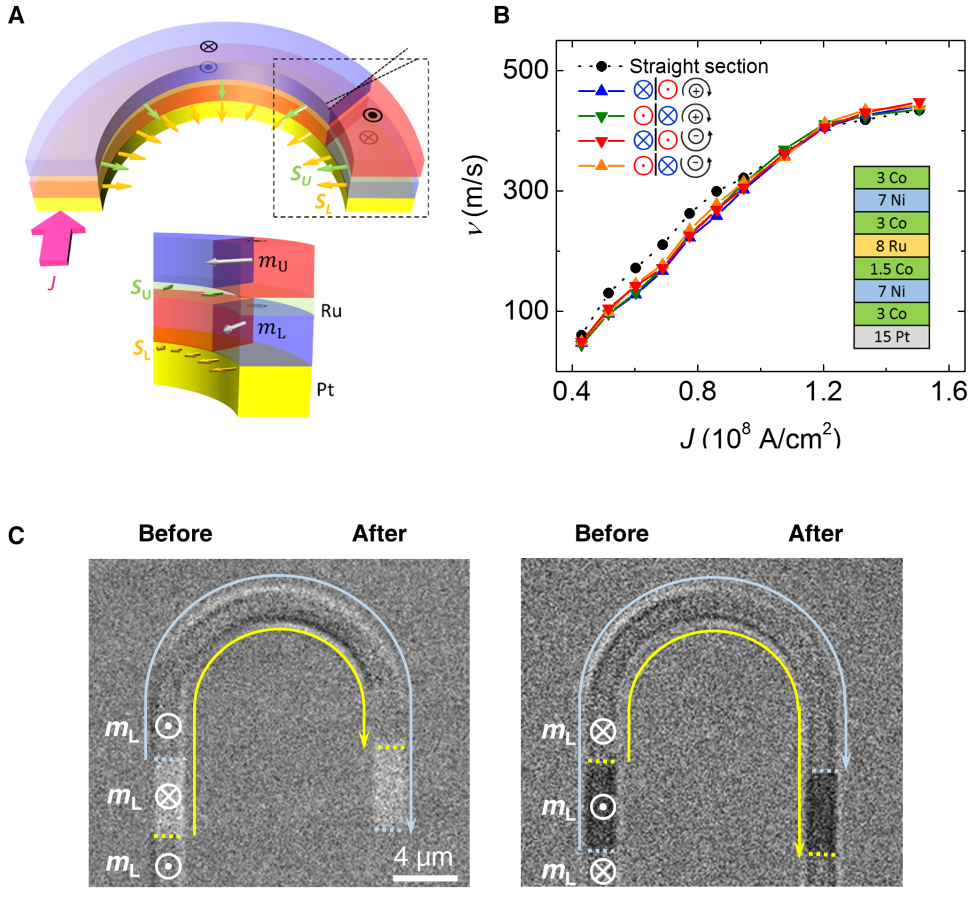

Fig. 4. DW motion along a curved wire in a SAF structure (**A**) Schematic illustration of the DW motion in a curved SAF nanowire showing the current-induced rotation of the Néel moments in the top (m_U) and bottom (m_L) layers by SHE from spin accumulation from the underlying Pt layer. (**B**) v versus J for ⊙ | ⊗ and ⊗ | ⊙ for positive and negative curvatures, respectively, for a device with R = 7 μm and w = 2 μm. The film stack is shown in the inset with thicknesses of layers in angstrom. (**C**) Representative Kerr images showing the motion of ⊙ | ⊗ | ⊙ and ⊗ | ⊙ | ⊗ DWs through a curved SAF nanowire.

exchange energy as the spin Hall torque rotates $\vec{m}$ away from $\vec{H}_{DM}$, which can be minimized by DW tilting. However, this lengthens the DW, thereby increasing the magnetostatic energy and limiting the DW tilt angle. In straight wires, the DW tilt angle should be constant across the wire (neglecting edge effects). However, in curved nanowires, this is not possible because the velocity of the DW at the outer rim must be higher than at the inner rim of the nanowire for steady-state motion of the DW. This means that the torque at the outer edge must be correspondingly larger and indeed must increase linearly from the inner to the outer rims. The fact that the current density is reduced at the outer rim compared to the inner rim accentuates the nonuniform tilting of the DW across the nanowire. Our quasi-2D model and micromagnetic simulations (*29*) confirm our conjecture (see the Supplementary Materials). The tilt, that is, the rotation of the DW can be in either the same or the opposite direction to the physical rotation of the wire itself (that is, curvature), leading to distinctive behaviors for opposite curvatures, as illustrated in Fig. 3. When the DW tilts away from the direction of the curvature, the chiral spin torque is decreased (Fig. 3A), and for the opposite curvature, the chiral spin torque is increased (Fig. 3B). In both cases, this is due to the increase or decrease of the angle between the $\vec{H}_{DM}$ and $\vec{m}$. In addition, $\vec{\tau}_k$ either adds or subtracts from $\vec{\tau}_{DM}$ depending on the curvature (see Fig. 3B), which is different from straight wires when $\vec{\tau}_k$ is always opposite to $\vec{\tau}_{DM}$.

The model also includes a periodic variation in the PMA field $\vec{H}_K$ along the wire to simulate DW pinning and thermal fluctuations in the DW position and magnetization (see the Supplementary Materials). Detailed results from the quasi-2D model that show the dependence of v and ϕ and ζon J are included in Fig. 3 (C to F). The model has features similar to our experimental results concerning the dependence of v on J, namely, a threshold J above which v gradually increases until v plateaus at different values for different curvatures and wire widths. Both ϕ and ζ reach plateaus at the same J as v, but whereas ζ takes very different values for different curvatures, ϕ is insensitive to the curvature. Thus, it is ζ that controls the dramatic dependence of the dynamical motion of the DW on curvature, as illustrated schematically in Fig. 3 (A and B). ζ has a nonmonotonic dependence on v that results from the DW pinning. Although it is clear that our model does not exactly match our experiments, it does account for the major features that we find and gives useful insight into their origin. The universal relationship between the DW speed and curvature that we find experimentally is reproduced by the model.

The model also shows how the influence of the curvature on the DW velocities is reduced as the nanowire width is reduced, as shown in Figs. 2 (D and E) and 3E. However, even for nanowires as narrow as 50 nm with the same ratio of radius of curvature to width as those shown in Fig. 2 (A and B), our model shows that there remains a pronounced difference in ⊙ | ⊗ and ⊗ | ⊙ DW velocities (see fig. S16).

One very important consequence of the curvature-dependent DW velocity is that, in the presence of curvature, ⊙ | ⊗ and ⊗ | ⊙ DWs move at different speeds: These speeds, as we have shown, can vary by an order of magnitude. This is a serious problem, which has not previously been appreciated, for DW devices such as racetrack memory (*5*) that rely on the lock-step motion of a series of DWs along a nanowire. However, we have discovered that the influence of the curvature is eliminated in synthetic antiferromagnetic (SAF) nanowires. Such SAF nanowires are composed of lower and upper magnetic layers that are coupled strongly antiferromagnetically via an ultrathin ruthenium layer (see the schematic structure in Fig. 4A) (*30*–*32*). Typical results for the DW velocity versus the current density for a SAF U-shaped device are shown in Fig. 4B. We note that, in agreement with our previous results for the CIDWM in SAF nanowires (*21*), the DW velocity is significantly higher in the SAF structure compared to single magnetic layer devices, both in the straight and in the curved sections. The DWs move at speeds of up to ~450 m/s compared to only ~150 m/s for the same current densities in single magnetic layer nanowires. The data in Fig. 4B clearly show that the DWs move at the same velocity independent of the curvature of the wire, and thus, the lock-step motion of a series of DWs is possible, as shown in Fig. 4C.

The insensitivity of the DW velocity on the curvature for SAF nanowires can be explained as follows. First, the DW tilting is largely suppressed in the SAF because the tilting of the ⊙ | ⊗ DW in one layer is opposite to that of the ⊗ | ⊙ DW in the other layer, and the strong antiferromagnetic coupling, therefore, mitigates tilting. Second, the CIDWM in the SAF nanowire is dominantly driven by an exchange-coupling torque (*21*) that is derived from the antiferromagnetic exchange coupling field that is much larger than both $\vec{H}_{DM}$ and $\vec{H}_{k}$. This torque depends only on the relative angle between the DW magnetizations in the lower and upper layers $\vec{m}_{L}$ and $\vec{m}_{U}$, which is independent of the DW configuration.

In summary, we have found that the velocity of DWs is significantly affected by the curvature of racetracks in which they are driven by current. Moreover, we find that there is a universal relationship between the increase or decrease of the DW's velocity to the direction in which the DWs move around the racetrack, independent of the sign of the SHE and DMI that provides the driving torques. In racetracks formed from synthetic antiferromagnets, the effect of the curvature is significantly diminished or eliminated, reinforcing the attractiveness of SAF racetracks for DW-based memory, logic, and sensor devices.

MATERIALS AND METHODS

Sample preparation

The thin film structures were grown using magnetron sputtering on Si(100) wafers on which an SiO_2 layer with a thickness of ~250 Å had been formed by thermal oxidation techniques. The magnetic structures were grown on top of the SiO_2 layer. Various underlayers and thicknesses and sequences of the magnetic layers were used, which allowed for tuning of the strength of the DMI at the top and bottom interfaces of the magnetic stack and the magnitude of the spin currents generated by SHE in heavy metal layers at the top and bottom interfaces of the magnetic stack. The magnetic stacks and the layers used to generate the spin currents via SHE are shown as insets in Fig. 1. For the structure shown in Fig. 1B, a seed layer of 100 Å AlO_x | 20 Å TaN was formed by first depositing a layer of AlO_x that was deposited by reactive magnetron sputtering using an Ar/O_2 (97/3) mixture onto the SiO_2 layer followed by a layer of TaN formed by reactive sputtering of Ta in an Ar/N_2 (90/10) mixture. For the structures shown in Fig. 1 (D and E), a seed layer of 100 Å AlO_x | 20 Å TaN was used. In all cases, a TaN capping layer of 50 Å was grown on top of the film stack shown in Fig. 1 to protect the film from exposure to the ambient atmosphere. Using photolithographic techniques and Ar ion milling, U-shaped nanowire devices were etched from the thin film stacks. These devices were protected by the deposition of an AlO_x layer of the same thickness as that of the film thickness in the etched-out region. The U-shaped devices were fabricated with large areas at either end of them that are used to make electrical contacts, as shown in Fig. 1A. Electrical contacts were made using aluminum wire bonds. The current density values indicated in our experiments correspond to the straight section of the U-shaped device.

Kerr microscopy

Kerr microscopy measurements to record DW motion were made in differential contrast mode using a Xenon light source. An image was taken of the current magnetization state of the device: This is digitally subtracted from subsequent images. Thus, subsequent changes in the magnetization state appeared as dark or bright regions, depending on whether the magnetization in those regions is increased or decreased, that is, an up-pointing region that becomes displaced by a down-pointing region appears as bright, and correspondingly, a down-pointing region that becomes displaced by an up-point region appears as a dark region.

DW injection

(1)To obtain a single DW: First, the device was magnetized in a single-domain state by applying a perpendicular magnetic field in a given direction that is larger than the coercive field. Next, a perpendicular magnetic field was applied in the opposite direction that is sufficient to cause nucleation of a domain in one of the pads. This field was turned off when the domain from the nucleated region enters the nanowire. The domain nucleated randomly in one of the pads, because of the much larger area of the pads compared to that of the wire.

(2)To obtain a pair of DWs: First, the device was magnetized in a single-domain state by the application of an out-of-plane field, and then the field was turned off. Next, an in-plane magnetic field was applied parallel to the straight sections of the U-shaped device. Then, an electrical pulse into the device was used to reverse the magnetization of one of the straight sections of the nanowire plus a part of the curved region via spin Hall torque[21,36]. An in-plane magnetic field varying from ~500 to 1,000 Oe was used with correspondingly smaller current pulses for the larger fields. Electrical pulses were then applied to bring the two DWs (one at one of the ends of the nanowire, and the other in the curved section) to specific positions for carrying out the experiments. The spacing between the pair of DWs was first adjusted by moving the DW in the curved portion of the nanowire toward the DW at the end of the wire, which was pinned because a much larger current density was needed to move this DW into the large pad. Then, the two DWs were moved together around the nanowire. Alternatively, the in-plane magnetic field can be applied perpendicular to the straight sections of the nanowire, and current pulses were then used to generate two DWs in the curved part of the nanowire. Last, a small permanent magnet was occasionally used in conjunction with the sequences of current pulses to generate two DWs.

The detailed DW velocity measurements presented in the paper were based on single DW studies. In these cases, a DW was initially positioned at a specific position inside the straight or curved section of the U-shaped device. The DW velocity was then determined by applying current pulses with lengths that were varied from 50 to 100 ns.

SUPPLEMENTARY MATERIALS

Supplementary material for this article is available at http://advances.sciencemag.org/cgi/content/full/3/5/e1602804/DC1

Supplementary Text

fig. S1. Schematic illustration of basic parameters used in the Q2D model for current driven domain wall motion.

fig. S2. Profile of anisotropy constant $K_{eff}(q)$ with $K^0_{eff} = 3.5 \times 10^6$ erg/cm^3, $\eta = 0.03$, $q_s = 0$ nm, and $q_0 = 10$ nm.

fig. S3. Modeling of thermal broadening.

fig. S4. Schematic of current distribution in curved wire with width w and mid-radius R.

fig. S5. Plots of Q2D model calculation results that take neither nonuniform current distribution nor pinning and thermal fluctuation into account.

fig. S6. Radial dependence of DW velocities transverse to the curve wire direction.

fig. S7. Plots of Q2D model calculation results that take pinning and thermal fluctuation but no nonuniform current distribution into account.

fig. S8. Plots of time-resolved Q2D model calculation results that take pinning and thermal fluctuation but no nonuniform current distribution into account.

fig. S9. Plots of Q2D model calculation results that take nonuniform current distribution and pinning, but no thermal fluctuation into account.

fig. S10. Plots of Q2D model calculation results that take nonuniform current distribution, pinning, and thermal fluctuation into account for various radii while width is fixed.

fig. S11. Plots of Q2D model calculation results that take nonuniform current distribution, pinning, and thermal fluctuation into account for various widths while the radius is fixed.

fig. S12. Plots of time-resolved Q2D model calculation results that take pinning and thermal fluctuation but no nonuniform current distribution into account.

fig. S13. Comparison of micromagnetic simulations and Q2D model.

fig. S14. Unabridged Kerr images corresponding to the main text.

fig. S15. Schematic table outlines the relationship between the effect of curvature on the DW velocity (⊙ | ⊗ or ⊗ | ⊙), which is found to be independent of the sign of DMI or SHE.

fig. S16. v against J of the quasi-2D model calculation results that take nonuniform current distribution, pinning, and thermal fluctuation into account for R = 100, 150, and 175 nm while w is fixed at 50 nm.

movie S1. Animation of Q2D calculation of time resolved DW motion in curved nanowires with positive curvatures for various radii and widths.

Reference (*33*–*36*)

REFERENCES AND NOTES

1. J. Slonczewski, Current driven excitation of magnetic multilayers. *J. Magn. Magn. Mater.* **159**, L1–L7 (1996).
2. D. C. Ralph, M. D. Stiles, Spin transfer torques. *J. Magn. Magn. Mater.* **320**, 1190–1216 (2008).
3. S. S. P. Parkin, X. Jiang, C. Kaiser, A. Panchula, K. Roche, M. Samant, Magnetically engineered spintronic sensors and memory. *Proc. IEEE* **91**, 661–680 (2003).
4. S. Ikeda, K. Miura, H. Yamamoto, K. Mizunuma, H. D. Gan, M. Endo, S. Kanai, J. Hayakawa, F. Matsukura, H. Ohno, A perpendicular-anisotropy CoFeB–MgO magnetic tunnel junction. *Nat. Mater.* **9**, 721–724 (2010).
5. S. S. P. Parkin, M. Hayashi, L. Thomas, Magnetic domain-wall racetrack memory. *Science* **320**, 190–194 (2008).
6. S. S. P. Parkin, Data in the fast lanes of racetrack memory. *Sci. Am.* **300**, 76–81 (2009).
7. M. Hayashi, L. Thomas, R. Moriya, C. Rettner, S. S. P. Parkin, Current-controlled magnetic domain-wall nanowire shift register. *Science* **320**, 209–211 (2008).
8. S. Fukami, T. Suzuki, K. Nagahara, N. Ohshima, Y. Ozaki, S. Saito, R. Nebashi, N. Sakimura, H. Honjo, K. Mori, C. Igarashi, S. Miura, N. Ishiwata, T. Sugibayashi, Low-current perpendicular domain wall motion cell for scalable high-speed MRAM, in *Symposium on VLSI Technology Digest of Technical Papers* (2009), pp. 230–231.
9. E. Saitoh, H. Miyajima, T. Yamaoka, G. Tatara, Current-induced resonance and mass determination of a single magnetic domain wall. *Nature* **432**, 203–206 (2004).
10. I. M. Miron, T. Moore, H. Szambolics, L. D. Buda-Prejbeanu, S. Auffret, B. Rodmacq, S. Pizzini, J. Vogel, M. Bonfim, A. Schuhl, G. Gaudin, Fast current-induced domain-wall motion controlled by the Rashba effect. *Nat. Mater.* **10**, 419–423 (2011).
11. A. V. Khvalkovskiy, V. Cros, D. Apalkov, V. Nikitin, M. Krounbi, K. A. Zvezdin, A. Anane, J. Grollier, A. Fert, Matching domain wall configuration and spin-orbit torques for very efficient domain-wall motion. *Phys. Rev. B* **87**, 020402 (2013).
12. L. Liu, O. J. Lee, T. J. Gudmundsen, D. C. Ralph, R. A. Buhrman, Current-induced switching of perpendicularly magnetized magnetic layers using spin torque from the spin Hall effect. *Phys. Rev. Lett.* **109**, 096602 (2012).
13. L. Liu, C.-F. Pai, Y. Li, H. W. Tseng, D. C. Ralph, R. A. Buhrman, Spin-torque switching with the giant spin Hall effect of tantalum. *Science* **336**, 555–558 (2012).
14. K.-S. Ryu, L. Thomas, S.-H. Yang, S. S. P. Parkin, Chiral spin torque at magnetic domain walls. *Nat. Nanotechnol.* **8**, 527–533 (2013).
15. S. Emori, U. Bauer, S.-M. Ahn, E. Martinez, G. S. D. Beach, Current-driven dynamics of chiral ferromagnetic domain walls. *Nat. Mater.* **12**, 611–616 (2013).
16. P. P. J. Haazen, E. Murè, J. H. Franken, R. Lavrijsen, H. J. M. Swagten, B. Koopmans, Domain wall depinning governed by the spin Hall effect. *Nat. Mater.* **12**, 299–303 (2013).
17. A. Thiaville, S. Rohart, E. Jué, V. Cros, A. Fert, Dynamics of Dzyaloshinskii domain walls in ultrathin magnetic films. *Europhys. Lett.* **100**, 57002 (2012).
18. J. Sampaio, V. Cros, S. Rohart, A. Thiaville, A. Fert, Nucleation, stability and current-induced motion of isolated magnetic skyrmions in nanostructures. *Nat. Nanotechnol.* **8**, 839–844 (2013).
19. W. Jiang, P. Upadhyaya, W. Zhang, G. Yu, M. B. Jungfleisch, F. Y. Fradin, J. E. Pearson, Y. Tserkovnyak, K. L. Wang, O. Heinonen, S. G. E. te Velthuis, A. Hoffmann, Blowing magnetic skyrmion bubbles. *Science* **349**, 283–286 (2015).
20. K.-S. Ryu, S.-H. Yang, L. Thomas, S. S. P. Parkin, Chiral spin torque arising from proximity induced magnetization. *Nat. Commun.* **5**, 3910 (2014).
21. S.-H. Yang, K.-S. Ryu, S. S. P. Parkin, Domain-wall velocities of up to 750 ms^{-1} driven by exchange-coupling torque in synthetic antiferromagnets. *Nat. Nanotechnol.* **10**, 221–226 (2015).
22. I. E. Dzyaloshinskii, Thermodynamic theory of weak ferromagnetism in antiferromagnetic substances. *J. Exp. Theor. Phys.* **5**, 1259–1272 (1957).
23. I. E. Dzyaloshinskii, Theory of helicoidal structures in antiferromagnets .I. Nonmetals. *J. Exp. Theor. Phys.* **19**, 960–971 (1964).
24. T. Moriya, Anisotropic superexchange interaction and weak ferromagnetism. *Phys. Rev.* **120**, 91–98 (1960).
25. K.-S. Ryu, S.-H. Yang, S. S. P. Parkin, Experimentally tunable chiral spin transfer torque in domain wall motion. *New J. Phys.* **18**, 053027 (2016).
26. A. P. Malozemoff, J. C. Slonczewski, *Magnetic Domain Walls in Bubble Material* (Academic, 1979).
27. K.-S. Ryu, L. Thomas, S.-H. Yang, S. S. P. Parkin, Current induced tilting of domain walls in high velocity motion along perpendicularly magnetized micron-sized Co/Ni/Co racetracks. *Appl. Phys. Express* **5**, 093006 (2012).
28. O. Boulle, S. Rohart, L. D. Buda-Prejbeanu, E. Jué, I. M. Miron, S. Pizzini, J. Vogel, G. Gaudin, A. Thiaville, Domain wall tilting in the presence of the Dzyaloshinskii-Moriya interaction in out-of-plane magnetized magnetic nanotracks. *Phys. Rev. Lett.* **111**, 217203 (2013).
29. LLG Micromagnetics Simulator, http://llgmicro.home.mindspring.com/
30. S. S. P. Parkin, N. More, K. P. Roche, Oscillations in exchange coupling and magnetoresistance in metallic superlattice structures: Co/Ru, Co/Cr and Fe/Cr. *Phys. Rev. Lett.* **64**, 2304–2307 (1990).
31. S. S. P. Parkin, D. Mauri, Spin-engineering: Direct determination of the RKKY far field range function in Ruthenium. *Phys. Rev. B* **44**, 7131 (1991).
32. S. S. P. Parkin, Systematic variation of the strength and oscillation period of indirect magnetic exchange coupling through the 3*d*, 4*d* and 5*d* transition metals. *Phys. Rev. Lett.* **67**, 3598–3601 (1991).
33. A. Thiaville, Y. Nakatani, J. Miltat, Y. Suzuki, Micromagnetic understanding of current-driven domain wall motion in patterned nanowires. *Europhys. Lett.* **69**, 990–996 (2005).
34. A. Capua, S.-H. Yang, T. Phung, S. S. P. Parkin, Determination of intrinsic damping of perpendicularly magnetized ultrathin films from time-resolved precessional magnetization measurements. *Phys. Rev. B* **92**, 224402 (2015).
35. S. Fukami, M. Yamanouchi, S. Ikeda, H. Ohno, Depinning probability of a magnetic domain wall in nanowires by spin-polarized currents. *Nat. Commun.* **4**, 2293 (2013).
36. A. Hubert, *Theorie der Domänenwände in Geordneten Medien* (Springer, 1974).

Acknowledgments: We thank B. Hughes for his help in device fabrication. **Funding:** We thank the Army Research Office (contract no. W911NF-13-1-0107) for their partial support of this work. **Author contributions:** All authors contributed to the conception of this study and discussed the results. C.G. designed the experiments and made the measurements. S.-H.Y. grew the films and carried out the analytical modeling. C.G. and T.P. did the micromagnetic simulations. C.G., S.-H.Y., and S.S.P.P. wrote the manuscript. S.S.P.P. supervised the study. **Competing interests:** The authors declare that they have no competing interests. **Data and materials availability:** All data needed to evaluate the conclusions in the paper are present in the paper and/or the Supplementary Materials. Additional data related to this paper may be requested from the authors.

Submitted 12 November 2016
Accepted 7 March 2017
Published 5 May 2017
10.1126/sciadv.1602804

Citation: C. Garg, S.-H. Yang, T. Phung, A. Pushp, S. S. P. Parkin, Dramatic influence of curvature of nanowire on chiral domain wall velocity. *Sci. Adv.* **3**, e1602804 (2017).